



Evaluation of Surface Layer Stability Functions and Their Extension to First Order Turbulent Closures for Weakly and Strongly Stratified Stable Boundary Layer

Andrey V. Debolskiy^{1,2,3}  · Evgeny V. Mortikov^{1,2,4} · Andrey V. Glazunov^{1,2,4} · Christof Lüpkes⁵

Received: 1 September 2021 / Accepted: 9 January 2023
© The Author(s), under exclusive licence to Springer Nature B.V. 2023

Abstract

In this study, we utilize a generalization of Monin–Obukhov similarity theory to construct first order turbulent closures for single-column models of the atmospheric boundary layer (ABL). A set of widely used universal functions for dimensionless gradients is evaluated. Two test cases based on Large-Eddy Simulations (LES) experimental setups are considered – weakly stable ABL (GABLS1; Beare et al. in Bound Layer Meteorol 118(2):247–272, 2006), and very strongly stratified ABL (van der Linden et al. in Bound Layer Meteorol 173(2):165–192, 2019). The comparison shows that approximations obtained using a linear dimensionless velocity gradient tend to match the LES data more closely. In particular, the EFB (Energy- and Flux- Budget) closure proposed by Zilitinkevich et al. (Bound Layer Meteorol 146(3):341–373, 2013) has the best performance for the tests considered here. We also test surface layer “bulk formulas” based on these universal functions. The same LES data are utilized for comparison. The setup showcases the behavior of surface scheme, when one assumes that the velocity and temperature profiles in ABL are represented correctly. The advantages and disadvantages of different surface schemes are revealed.

Keywords Large-eddy simulation · Monin–Obukhov similarity theory · Stable boundary layer · Turbulence closures

✉ Andrey V. Debolskiy
and.debol@gmail.com

¹ Lomonosov Moscow State University, Moscow, Russia

² Moscow Center for Fundamental and Applied Mathematics, Moscow, Russia

³ A.M. Obukhov Institute of Atmospheric Physics RAS, Moscow, Russia

⁴ Marchuk Institute of Numerical Mathematics RAS, Moscow, Russia

⁵ Alfred-Wegener-Institut Helmholtz-Zentrum für Polar- und Meeresforschung, Bremerhaven, Germany

1 Introduction

According to Monin–Obukhov similarity theory (MOST), in the stratified surface layer of the atmosphere, the vertical gradients of the mean velocity and scalars are related to the turbulent fluxes of these quantities and the distance to the surface z in a universal manner (Monin and Yaglom 1971). The stability parameter $\zeta = z/L$, where L is the Obukhov length scale, is the only dimensionless parameter that determines the type of flux-gradient relations. Universal functions of this parameter are introduced into MOST, which specify dimensionless gradients of velocity $\Phi_m(\zeta)$ and buoyancy $\Phi_h(\zeta)$. Through these gradients and the parameter ζ , it is possible to express unambiguously other dimensionless characteristics of the steady flow, such as dimensionless coefficients of turbulent viscosity and diffusivity, dimensionless scales of the Prandtl mixing length for momentum and scalars, turbulent Prandtl number, flux and gradient Richardson numbers, etc.

The most common object of MOST's application is the calculation of turbulent fluxes near the surface with known values of mean meteorological variables at a certain specified height z_m and known properties of the surface itself. In this case, the integration of universal gradients over z is performed, and the integration constants are associated with some conditional scales of length z_0 and z_{0t} (dynamic and thermal roughness lengths, determined empirically for surfaces of different types), which are much smaller than the height of z_m . This use of MOST leads to the well-known “bulk formulas” for calculating the coefficients of momentum, heat and moisture exchange between the surface and the atmosphere.

One generalization of MOST to turbulent flows with variable distribution of momentum and buoyancy fluxes with height is the local scaling (Nieuwstadt 1984; Gryanik et al. 2020). In this case, a first order closures can be constructed from universal functions for dimensionless velocity and temperature gradients.

The set of universal functions proposed in the literature is currently quite large. They differ in both coefficients and functional dependence on the stability parameter ζ , which stems from both underlying assumptions on asymptotic behavior and methods with which they are obtained. Moreover, the MOST is based on a number of assumptions, not all of which can be fulfilled in the practical application of this theory to surface flux schemes and PBL parameterizations. In particular, for stable stratification, the assumption about the presence of a constant flux layer is significantly violated already for heights at which the first levels of large-scale atmospheric models are located. Accordingly, the functions used in the models cannot be fully universal and introduce different errors depending on the meteorological situation and the way these functions are applied. In fact, all these functions have a limited range of applicability, and it is quite possible that some of them are more suitable for local one-dimensional closures, while the others are more suitable for obtaining bulk formulas for evaluation (calculation) of surface fluxes on coarse computational grids, common for numerical models of climate and weather forecast.

In this paper, we will try to compare various universal functions from this point of view. Universal functions for dimensionless gradients proposed by different authors will be used to construct single-column models with first order local turbulent closures, and to derive bulk formulas under the assumption of constant flux layer. We compile a diverse set that includes functions with different asymptotic behavior and underlying assumptions as well as frequently used ones. The results are compared with data from LES experiments.

As one example, the simulations of a stable ABL according to the GABLS1 experiment setup (Beare et al. 2006) are considered. This scenario has been used many times to test LES models and their subgrid closures (e.g. Basu and Porté-Agel 2006), and has also been

performed at very high spatial resolution (Sullivan et al. 2016). In addition, this scenario has repeatedly demonstrated the convergence of the LES results to a single solution (with some exceptions; see, Maronga and Li 2022) when refining model grids. Therefore, we have every reason to believe that large-eddy simulations according to the GABLS1 setup adequately reflect the physics of the phenomenon under consideration, and their results can be considered as the best reference data for testing turbulent closures performance in weakly stable stratification. Previously, this setup has often been used (Svensson and Holtslag 2009; Pleim et al. 2010; Sterk et al. 2012; Holtslag et al. 2013) for intercomparison and validation of single-column numerical boundary layer models with LES data. In this paper, in addition to the LES results of Beare et al. (2006), we will use results obtained with two different LES models described in (Glazunov et al. 2016, INM-LES—Institute of Numerical Mathematics LES) and (Tkachenko et al. 2021; Kadantsev et al. 2021, DSLA-LES—Dynamic Smagorinsky Lagrangian Averaging LES), which use different subgrid closures and numerical schemes.

For testing of closures and surface schemes in the regime of a very stable boundary layer (VSBL), the LES experiments obtained by van der Linden et al. (2019) are used. This experiment is based on field observation data at the Antarctic station Dome C (Genthon et al. 2013). The simulations were carried out with fine grid resolution and rapid surface cooling (16 times faster than in GABLS1), which led to the formation of an ABL with a thickness of about 6 meters, which is the same order of magnitude as stable ABL in the Arctic (Grachev et al. 2007; Petenko et al. 2019). Note that another example of similar setup is the GABLS4 case (Couvreur et al. 2020), which was performed with the coarser resolution of the LES models, as evidenced by the large spread of their results. Also VSBL setup includes the effect of large-scale subsidence and a period of constant surface temperature, which lead to different shapes of profiles for temperature and heat flux. In addition to LES data from van der Linden et al. (2019) we performed our own simulations for VSBL case with DSLA-LES model, which is based on the dynamic Lagrangian-averaged Smagorinsky subgrid closure proposed by Meneveau et al. (1996).

Note that this study does not consider the possible effects associated with the heterogeneity of the underlying surface and with the radiation forcing distributed over the ABL thickness. These effects may well change the form of the considered universal functions. In our opinion, this dependence should be the topic of separate studies.

The paper is structured as follows. In Sect. 2, we review the basic assumptions of MOST and its extensions and applications. In Sect. 3, we explain how first order closures are constructed from local generalization of MOST and introduce the set of universal functions for dimensionless gradients we intend to test. In Sect. 4, we proceed to compare the performance of constructed first order closures and their surface scheme counterparts against LES data. This is followed by summary and conclusions in Sect. 5.

2 Monin–Obukhov Similarity Theory and Its Applications

Initially (Monin and Yaglom 1971), MOST was constructed with the assumptions of the statistical stationarity of the flows and the smallness of changes in turbulent fluxes with height within a certain layer, often called surface layer. However, in its practical application in large-scale atmospheric circulation models or for indirect measurements of surface fluxes, these assumptions often turn out to be violated. An example of the use of MOST in conditions it is not intended for is the modeling of a strongly stable, and, therefore, rather small in thickness, atmospheric boundary layer on coarse grids of large-scale atmospheric models.

In most global atmospheric models, the first model level is often located at heights of ~ 10 meters above the surface, which is comparable to the characteristic thickness of the shallow stable ABL, which can occur in winter conditions at high latitudes (Grachev et al. 2007; Esau 2008; Petenko et al. 2019). For an ABL in a quasi-equilibrium state, developing with constant surface cooling in the absence of internal sources, the turbulent heat flux decreases linearly in the vertical direction: $F_z(z) \approx F_z(0)(1 - \eta)$ (here, $\eta = z/h$ and h is the ABL height), and the momentum flux decreases even faster: $\tau(z) \approx \tau(0)(1 - \eta)^{3/2}$ (Nieuwstadt 1984). Thus, the assumption that the fluxes are constant with height can be violated by a factor of two or more if the first model grid node center is in the middle of the ABL.

It is common that not only the thin surface layer, but the entire ABL can be considered in a quasi-equilibrium state (Nieuwstadt 1984; Derbyshire 1999), which allows generalizing the similarity theory to its entire thickness. When constructing such a scaling, in addition to the stability parameter $\zeta = z/L$, the dimensionless height $\eta = z/h$ should be a key parameter characterizing the turbulent length scales. A classic example of an alternative approach to MOST scaling is the Deardorff similarity theory (Deardorff 1970), where the height h acts as the only length scale for the convective ABL, which uniquely determines all flow characteristics in the absence of vertical wind shear. The inclusion of the Deardorff convective velocity scale $w_* = (\beta F_z(0)h)^{1/3}$ in the bulk formulas when calculating surface fluxes, which is widespread in the models of the surface layer, can be considered as an example of the hybrid use of MOST and Deardorff scaling. Another approach for introducing η into the scaling is discussed by Emeis (2014).

In empirical universal functions of dimensionless velocity and temperature gradients for stable stratification, the dependence on the dimensionless height z/h can be implicitly present. This is due to the fact that the height h and the Obukhov length scale near the surface, L , turn out to be proportional to each other: $h/L \sim 2-4$ under typical conditions for the development of a stable ABL. Note that this proportionality is approximate and does not completely cancel the dependence of h/L on the ABL evolution prehistory and some external parameters, for example, on the value of f/N , where f is the Coriolis parameter, and N is the Brunt–Väisälä frequency in free atmosphere above boundary layer (see, e.g., Zilitinkevich and Baklanov 2002). To obtain from observations functions $\tilde{\Phi}(z/L)$ and $\tilde{\Phi}(z/L)$, which are dependent only on one parameter, one just needs to measure the fluxes and the scale L near the surface, and the gradients at height z . Then the typical dependence of the fluxes on the parameter $\eta = z/h \sim \zeta = z/L$ will determine the form of these functions, and they can be used in the same way as the dimensionless gradients in the original MOST.

An example of linear approximation of the functions $\tilde{\Phi}_h(\zeta)$ and $\tilde{\Phi}_m(\zeta)$ are the well-known Businger-Dyer functions (Dyer 1974), which, due to the successful choice of four constants (including the Prandtl number at the surface and the von Karman constant) practically coincide with the dimensionless gradients scaled in the above-described way according to LES results up to heights of $z \sim \frac{1}{3}h$, where the turbulent momentum flux decreases by almost a factor of two in comparison with its surface value (see, functions $\Phi_h(z/L)$ and $\Phi_m(z/L)$ shown in additional materials to (Beare et al. 2006) at <https://gabls.metoffice.com> and, also, Fig. 7 from Glazunov (2014a)). Implicitly accounting for the vertical distribution of momentum and buoyancy fluxes in empirical approximations of dimensionless gradients makes it possible to use bulk formulas to obtain correct estimates of flux values at the surface for relatively high z/h . At the same time, these bulk formulas will provide incorrect flux profiles.

Another example of MOST generalization to turbulent flows with height-variable momentum and buoyancy fluxes is the local scaling proposed by Nieuwstadt (1984). With this scaling, the dimensionless gradients $\phi_m(z/\Lambda)$ and $\phi_h(z/\Lambda)$ are considered universal throughout the

whole ABL. Here, the local Obukhov scale $\Lambda(z)$ is used, calculated from the values of fluxes at the same height where the flux-gradient relation is established (in our notation: $\Lambda(z=0) \equiv L$). Local scaling is convenient for constructing turbulence closures for one-dimensional ABL models. For example, in Mortikov et al. (2019) it was shown that using the relaxation of the turbulent wave number scale to the value defined by $\phi_m(z/\Lambda)$, one can obtain turbulence closure very similar to the classical $k - \varepsilon$ model, and, at the same time, reduce the number of semi-empirical constants in the dissipation equation from four to one.

The local scaling has one significant shortcoming: when it is used, the dependence of the universal functions on the parameter $\eta = z/h$ is completely lost. Because of the limited turbulent length scales under stable stratification, the influence of the upper ABL boundary on the processes at the surface and in the interior of the ABL is relatively small. However, in the upper part of ABL, significant fractions of the momentum and heat is transported by relatively large eddies generated non-locally, and the integral length scales h and $L \gg \Lambda(z)$, responsible for the static stability of the flow as a whole, become important again (Glazunov 2014b). Because of the increasing turbulent length scales relative to Λ , at the top of the ABL, the dimensionless gradient of velocity $\phi_m(z/\Lambda)$ grows slower than linearly, and the dimensionless gradient for the temperature $\phi_h(z/\Lambda)$ grows slower than that of velocity, so formally defined Prandtl number $\text{Pr}_t = \phi_h/\phi_m$ is reduced. This happens because of the features of the mean flow and since the turbulent fluxes are not directly related to local gradients. The described behavior is typical for the turbulent Ekman layer and turns out to be non-universal when the parameters of the external dynamic forcing change (see, Glazunov 2014a, b).

Most studies devoted to the experimental determination of dimensionless gradients do not focus on the differences between local scaling and scaling to near-surface turbulent scales, it is implicitly assumed that: $\phi_{m,h} \approx \Phi_{m,h} \approx \hat{\Phi}_{m,h}$ (this, generally speaking, is true only within the “constant flux” layer). When constructing single column ABL models and when obtaining bulk formulas, the same universal dependencies are most often used. This can lead to significant errors. Dimensionless gradients are empirical functions and are determined from a large set of field data with high uncertainty. For example, if measurements were carried out, including at heights comparable to the thickness of the ABL, which can occur for most measurements at high latitudes, then the resulting empirical dependence will inevitably be characterized by underestimated Prandtl numbers and overestimated length scales in comparison with what is necessary for successful local one-dimensional modeling of the ABL. On the other hand, the local dimensionless gradients $\phi_{m,h}(z/\Lambda)$, measured in the lower and middle parts of the ABL, may turn out to be suitable for local one-dimensional models, but inapplicable for bulk formulas obtained under the assumption of height-independent fluxes.

3 First Order Closures with Local Scaling and Dimensionless Gradient Functions

We proceed with constructing locally scaled first order turbulent closures. For one-dimensional ABL models governing equations for mean velocity and temperature are obtained from Reynolds-averaged Navier–Stokes equations simplified by horizontal homogeneity assumption leaving only the dependence on vertical coordinate z :

$$\frac{\partial U}{\partial t} + \frac{\partial \tau_x}{\partial z} = f(V - V_g) - w_{\text{sub}} \frac{\partial U}{\partial z}, \quad (1)$$

$$\frac{\partial V}{\partial t} + \frac{\partial \tau_y}{\partial z} = -f(U - U_g) - w_{\text{sub}} \frac{\partial V}{\partial z}, \tag{2}$$

$$\frac{\partial \theta}{\partial t} + \frac{\partial F_z}{\partial z} = -w_{\text{sub}} \frac{\partial \theta}{\partial z}, \tag{3}$$

where U and V are horizontal components of mean velocity vector \mathbf{U} , $\tau_x = \overline{u'w'}$, $\tau_y = \overline{v'w'}$ are components of vertical turbulent momentum flux τ , θ is potential temperature, $F_z = \overline{\theta'w'}$ is vertical turbulent heat flux, f is the Coriolis parameter, U_g, V_g are geostrophic wind components, $w_{\text{sub}} = -\int_0^z \left(\frac{\partial U}{\partial x} + \frac{\partial V}{\partial y} \right) dz$ is vertical subsidence velocity due to large-scale divergence. Turbulent fluxes are expressed through gradient approximation:

$$\tau = -K_m \frac{\partial \mathbf{U}}{\partial z}, F_z = -K_h \frac{\partial \theta}{\partial z}. \tag{4}$$

In first order closures, turbulent viscosity and diffusivity are given as:

$$K_m = f_m l^2 \left| \frac{\partial \mathbf{U}}{\partial z} \right|, \tag{5}$$

$$K_h = f_h l^2 \left| \frac{\partial \mathbf{U}}{\partial z} \right|, \tag{6}$$

where $f_{m,h}$ are normalized transfer coefficients for momentum and heat, $\left| \frac{\partial \mathbf{U}}{\partial z} \right| = \sqrt{\left(\frac{\partial U}{\partial z} \right)^2 + \left(\frac{\partial V}{\partial z} \right)^2}$, l is turbulent length scale for neutral conditions, $l \sim \kappa z$. Local flux-gradient relations can be expressed as:

$$\frac{\partial \mathbf{U}}{\partial z} = \frac{-\tau \phi_m(\zeta)}{\sqrt{\tau} \kappa z}, \tag{7}$$

$$\frac{\partial \theta}{\partial z} = \frac{\theta_*}{\kappa z} \phi_h(\zeta), \tag{8}$$

where $\theta_* = -\frac{F_z}{u_*}$ is the turbulent temperature scale, F_z is the turbulent heat flux, κ is the von Karman constant, $\zeta = \frac{z}{\Lambda}$ is the local stability parameter, $\Lambda = \frac{u_*^2}{\beta \kappa \theta_*}$ is the local Obukhov length scale, $u_* = \sqrt{\tau}$ is friction velocity and $\tau = |\tau|$, $\beta = \frac{g}{\theta_0}$ is buoyancy parameter with g as acceleration of gravity and θ_0 as reference potential temperature, and $\phi_{m,h}$ are universal functions for dimensionless velocity and temperature gradients. The functions $\phi_{m,h}$ can be related to normalized transfer coefficients as:

$$f_m = \phi_m^{-2}(\zeta), \tag{9}$$

$$f_h = \frac{1}{\phi_m(\zeta) \phi_h(\zeta)}. \tag{10}$$

The turbulent Prandtl number Pr_t , flux Richardson number Ri_f , and gradient Richardson number Ri_g in such a closure can be expressed as:

$$Pr_t = \frac{K_m}{K_h} = \frac{\phi_h}{\phi_m}, \tag{11}$$

$$Ri_f = \frac{\beta F_z}{\tau_x \frac{\partial U}{\partial z} + \tau_y \frac{\partial V}{\partial z}} = \frac{\beta \theta_* \kappa z}{u_*^2} \phi_m^{-1} = \frac{\zeta}{\phi_m}, \tag{12}$$

$$Ri_g = \frac{\beta \frac{\partial \theta}{\partial z}}{\left| \frac{\partial \mathbf{U}}{\partial z} \right|^2} = \frac{\beta \theta_* \kappa z}{u_*^2} \frac{\phi_h}{\phi_m^2} = \frac{\zeta \phi_h}{\phi_m^2}. \tag{13}$$

For the solution of the system [Eqs. (1)–(10)], one need to express ζ through mean velocity and temperature profiles, using Eq. (13), either explicitly or by iterative procedure.

3.1 Linear Dimensionless Gradients

In classic Monin–Obukhov theory for stable turbulent surface layer Monin and Yaglom (1971) assume linear form of dimensionless gradients:

$$\phi_m = 1 + C_m \zeta, \tag{14}$$

$$\phi_h = Pr_{t0} (1 + C_h \zeta), \tag{15}$$

where Pr_{t0} is the Prandtl number for neutral stratification. Using (12) one can show how constant C_m governs the critical flux Richardson number:

$$Ri_f = \frac{\zeta}{1 + C_m \zeta} = C_m^{-1} - \frac{C_m^{-1}}{1 + C_m \zeta}, \tag{16}$$

$$\lim_{\zeta \rightarrow \infty} Ri_f = C_m^{-1}. \tag{17}$$

The range of constant $C_m \in [4.0, 5.5]$ corresponds to critical flux Richardson number of $Ri_{fc} \in [0.18, 0.25]$, which is well established in experimental data and observations (Monin and Yaglom 1971; Zilitinkevich et al. 2013, 2019). Equations (14) and (15) substituted into Eq. (13) result in a quadratic equation for ζ as a function of Ri_g , which has a positive root for $0 \leq Ri_g \leq Ri_{gc}$, where:

$$Ri_{gc} = \frac{Pr_{t0} C_h}{C_m^2}. \tag{18}$$

Depending on $\frac{C_h}{C_m}$ ratio, Pr_t for this solution increases or decreases up to $Pr_{tc} = \frac{Pr_{t0} C_h}{C_m}$ with $\zeta \rightarrow \infty$.

3.2 Turbulent Prandtl Number Parametrizations $Pr_t (Ri_g)$

The non-linear dimensionless temperature gradient ϕ_h may appear if an empirical $Pr_t (Ri_g)$ dependence is introduced, for example from Schumann and Gerz (1995):

$$Pr_t (Ri_g) = Pr_{t0} \left(\exp \left(\frac{-Ri_g}{Pr_{t0} Ri_{fc}} \right) + \frac{Ri_g}{Pr_{t0} Ri_{fc}} \right). \tag{19}$$

In this case, the dimensionless velocity gradient is still undefined and should be introduced. We will use a linear dimensionless velocity gradient (14), since some works (e.g., Zilitinkevich et al. 2019) show that the turbulent scales derived from it are in good agreement with the DNS (Direct Numerical Simulation) data of stably stratified turbulent Couette flow (Mortikov et al. 2019; Glazunov et al. 2019), and in addition, it allows the closure to obey the asymptotic of the bounded flux Richardson number under strong stability (Eq. (17)). Substituting Eq. (7) into Eq. (11) for ϕ_h :

$$\phi_h = Pr_t (Ri_g) \phi_m = Pr_t (Ri_g) (1 + C_m \zeta). \tag{20}$$

Substituting Eq. (20) to Eq. (13) gives:

$$Ri_g = \frac{\zeta Pr_t(Ri_g)}{(1 + C_m \zeta)}, \tag{21}$$

which can be solved for ζ with:

$$\zeta = \frac{Ri_g}{Pr_t(Ri_g) - C_m Ri_g}. \tag{22}$$

Note, that for some Ri_g , $C_m Ri_g > Pr_t(Ri_g)$, there is a critical gradient Richardson number for this form of dimensionless temperature gradient.

3.3 Energy- and Flux-Budget Closure

In the EFB (Energy- and Flux-Budget) closure (Zilitinkevich et al. 2013) it is assumed that a linear dimensionless velocity gradient is governing the equilibrium state of turbulent kinetic energy budget and thus turbulence may be maintained by shear at any stability. The turbulent Prandtl number is assumed to increase linearly with Ri_g at high stability and a set of other assumptions (e.g., on the relations between turbulent kinetic energy and potential energy dissipation; form of turbulent kinetic energy anisotropy $A_z = \overline{w'^2} / (\overline{w'^2} + \overline{u'^2} + \overline{v'^2})$ dependence on stability) is utilized. In its simplest form derived from steady state analysis, the closure can be reduced to a turbulent Prandtl number of the following form:

$$Pr_t = \frac{C_\tau}{C_F} / \left(1 + C_\nabla - (1 - C_\theta) \frac{C_P Ri_f}{A_z (1 - Ri_f)} \right). \tag{23}$$

Using $Ri_f(\zeta)$ from Eq. (16) and a linear dimensionless velocity gradient, Eq. (14), the following expression for $Pr_t(\zeta)$ can be obtained:

$$Pr_t = \frac{C_\tau}{C_F} / \left(C_2 - C_1 \frac{\zeta \left(1 + \frac{C_a}{A_{z\infty}} \zeta \right)}{(A_{z0} + C_a \zeta) (1 + (C_m - 1) \zeta)} \right), \tag{24}$$

where $C_2 = 1 + C_\nabla$, $C_1 = (1 - C_\theta) C_P$ and C_a is a constant. This can be further reduced to cubic equation for ζ with known Ri_g , for details see Appendix 1.

3.4 Non-linear Dimensionless Gradients

Following Grachev et al. (2007, 2008) and Gryanik et al. (2020) one can use two similar sets of stability functions with non-linear dimensionless velocity gradient:

$$\phi_m^{GA08}(\zeta) = 1 + a_{m1} \frac{\zeta (1 + \zeta)^{\frac{1}{3}}}{1 + b_{m1} \zeta}, \tag{25}$$

$$\phi_h^{GA08}(\zeta) = 1 + \frac{a_{h1} \zeta + b_{h1} \zeta^2}{1 + c_h \zeta + \zeta^2}, \tag{26}$$

and:

$$\phi_m^{GL20}(\zeta) = 1 + \frac{a_{m2} \zeta}{(1 + b_{m2} \zeta)^{\frac{2}{3}}}, \tag{27}$$

$$\phi_h^{GL20}(\zeta) = \text{Pr}_{t0} \left(1 + \frac{a_{h2}\zeta}{1 + b_{h2}\zeta} \right). \tag{28}$$

These empirical functions were derived from SHEBA (Surface Heat Budget of the Arctic Ocean Experiment) measurements, and are initially intended to be used in surface schemes (see Gryanik and Lüpkes (2022) for comprehensive package of these and other functions). The form for both velocity gradients approximations here is based on assumption of frictionless or “z-less” scaling, such that shear is independent of the friction velocity u_* in the limit of very strong stability, see (Grachev et al. 2007). Another asymptotic behavior assumed in those functions is that $\phi_h(\zeta)$ becomes constant for very high stability. Both pairs of universal functions imply that the Prandtl number goes to zero at large values of ζ .

Using similar assumptions, but making both $\phi_m(\zeta)$ and $\phi_h(\zeta)$ approach constant non-zero value at high ζ , another set of stability functions with non-linear dimensionless velocity gradient was obtained by Cheng and Brutsaert (2005), using CASES-99 field data:

$$\phi_m^{CB05} = 1 + a \left(\frac{\zeta + \zeta^b (1 + \zeta^b)^{\frac{1-b}{b}}}{\zeta + (1 + \zeta^b)^{\frac{1}{b}}} \right), \tag{29}$$

$$\phi_h^{CB05} = 1 + c \left(\frac{\zeta + \zeta^d (1 + \zeta^d)^{\frac{1-d}{d}}}{\zeta + (1 + \zeta^d)^{\frac{1}{d}}} \right). \tag{30}$$

Lastly we introduce probably the most frequently used functions of dimensionless gradients, at least in the past, and which are currently still in use in some climate and weather forecast models (Dufresne et al. 2013; Voltaire et al. 2013; Volodin et al. 2017), proposed in Louis (1979), Louis et al. (1982). They show a non-linear dependence of the dimensionless velocity gradient on stability. The reason for the popularity of the Louis closure in weather and climate forecast models is that it is easy to implement. Another factor is that for coarse vertical grids, this closure does not allow turbulent mixing to vanish even with very strong stability thus preventing decoupling of the ABL. As a consequence the Louis scheme almost always greatly overestimates mixing (Garratt et al. 2020). The stability functions in this closure are written as dependent on the gradient Richardson: number:

$$f_m = \frac{1}{1 + 10Ri_g (1 + 5Ri_g)^{-\frac{1}{2}}}, \tag{31}$$

$$f_h = \frac{1}{1 + 15Ri_g (1 + 5Ri_g)^{\frac{1}{2}}}. \tag{32}$$

Equations (9) and (10) allow to relate these stability functions to dimensionless gradients, and in this case the latter are only dependent on Ri_g :

$$\phi_m^{L79} = \sqrt{1 + 10Ri_g (1 + 5Ri_g)^{-\frac{1}{2}}}, \tag{33}$$

$$\phi_h^{L79} = \frac{1 + 15Ri_g (1 + 5Ri_g)^{\frac{1}{2}}}{\sqrt{1 + 10Ri_g (1 + 5Ri_g)^{-\frac{1}{2}}}}. \tag{34}$$

Table 1 Turbulence closures for comparison and legend key

| Name | $\phi_m(\zeta)$ | $\phi_h(\zeta)$ | References |
|------|-----------------|--------------------|--|
| BD71 | Eq. (14) | Eq. (15) | Businger et al. (1971), Dyer (1974) |
| EFB | Eq. (14) | Eqs. (24) and (11) | Zilitinkevich et al. (2013) |
| SG95 | Eq. (14) | Eqs. (19) and (22) | Schumann and Gerz (1995) |
| GA08 | Eq. (25) | Eq. (26) | Grachev et al. (2007), Grachev et al. (2008) |
| GL20 | Eq. (27) | Eq. (28) | Gryanik et al. (2020) |
| CB05 | Eq. (29) | Eq. (30) | Cheng and Brutsaert (2005) |
| L79 | Eq. (33) | Eq. (33) | Louis (1979), Louis et al. (1982) |

4 Comparison

In this section we provide a brief overview of the sets of universal functions introduced before and highlight differences between them.

For convenience, Table 1 summarizes the designation of closures used in figures and the forms of dimensionless gradients from which they are obtained. Later in the text we will refer to first order closures based on the locally generalized Monin–Obukhov theory (that is with local scaling z/Λ) which use particular stability functions.

To ease the comparison of one-dimensional models with each other, for all used closures, the most common identical set of constants was used, such as wherever possible we set the neutral Prandtl number and von Karman constant to the values obtained by LES data in experiments, while the “internal” constants for the universal functions are kept as in original formulations. Other constants, defined by the particular form of stability functions are set to values, which were originally proposed by the authors. According to our tests the best overall fit was achieved with $Pr_{t0} = 0.75$ and $\kappa = 0.4$.

Figure 1 shows the behaviour of the considered closures as well as data obtained from LES experiments with GABLS1 and VSBL setup. Note that hereafter data calculated from LES uses total (resolved + “subgrid”) fluxes. The LES and first order closures data appear to coincide in the near-neutral conditions, except for $Ri_g < 0.04$ for which wide spread in LES can be observed because the near surface flow is not well resolved. The spread both in LES data and between closures increases with stability. The largest differences appear in the region of $Ri_g > 0.17$ for both ϕ_m and ϕ_h , which corresponds to the upper half of the boundary layer in the VSBL experiment and upper quarter in the GABLS1 case. This can indicate that there is no universal behavior of dimensionless gradients in this part of the SBL and it might depend on the flow conditions and external forcing and a plethora of processes which occur at the interface of the ABL and the free atmosphere (intermittency, internal gravity waves – turbulence interactions etc.) as discussed in Sect. 2.

The closest match to the aggregated LES data for both dimensionless gradients in the region $0.1 < Ri_g < 0.17$ as seen in Fig. 1 is demonstrated by the BD71 functions, followed by the EFB and the GL20 closures. As will be evident in the following sections, this allows these closures to reproduce the mean profiles similar to those in LES. The region $Ri_g > 0.2$ appears in the upper part of SBL where the values of the momentum and heat fluxes are relatively small and thus will have less influence on the mean profiles. It can be noted that the solutions for SG95 and EFB closures give a similar linear growth of ζ for $Ri_g > 0.2$, where $Pr_t \sim C_m(Ri_g)$, and their Prandtl number behaviour is within bounds estimated in Basu and Holtslag (2021).

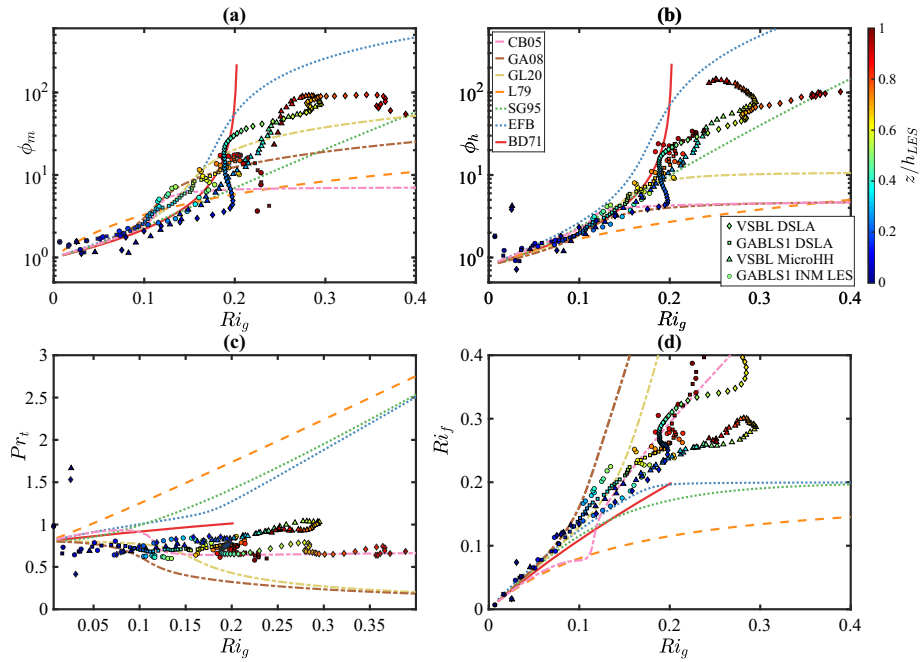


Fig. 1 **a** ϕ_m , **b** ϕ_h , **c** Pr_t , **d** Ri_f as functions of Ri_g . For legend see Table 1. The circles, triangles, diamonds and square points refer to LES data and are colour-coded (see colour bar on the top right of the Figure) according to the height z/h at which they are calculated

Solutions from closures constructed from SHEBA data significantly differ from other closures in their behavior. They do not show the presence of a critical flux Richardson number in their solution, and as a result of (see Eq. (11)) the turbulent Prandtl number does not increase with increasing stability, but decreases, which seems to contradict a number of studies (Schumann and Gerz 1995; Stretch et al. 2001; Zilitinkevich et al. 2013; Katul et al. 2014; Zilitinkevich et al. 2019). L79 closure significantly underestimates critical flux Richardson number, and a linear growth of the turbulent Prandtl number begins much earlier than in the SG95 or EFB closures.

4.1 Weakly Stable Boundary Layer Case

We will compare performance of obtained closures using the experimental setup GABLS1 (Cuxart et al. 2006). The single-column models were ran with the same resolution as LES. We include the results of two LES models with 3.25 m vertical resolution, which reproduced vertical distribution of mean wind velocity and temperature very close to the mean of GABLS1: INM LES model Glazunov et al. (2016) and LES-DSLA (Tkachenko et al. 2021; Kadantsev et al. 2021). The main difference of these models is in subgrid closure procedure: INM LES utilizes dynamic mixed Smagorinsky and scale similarity closure, while LES-DSLA uses dynamic approach supplemented with Lagrangian averaging to calculate Smagorinsky constant and subgrid Prandtl number. Despite those differences models perform very similar in the GABLS1 case.

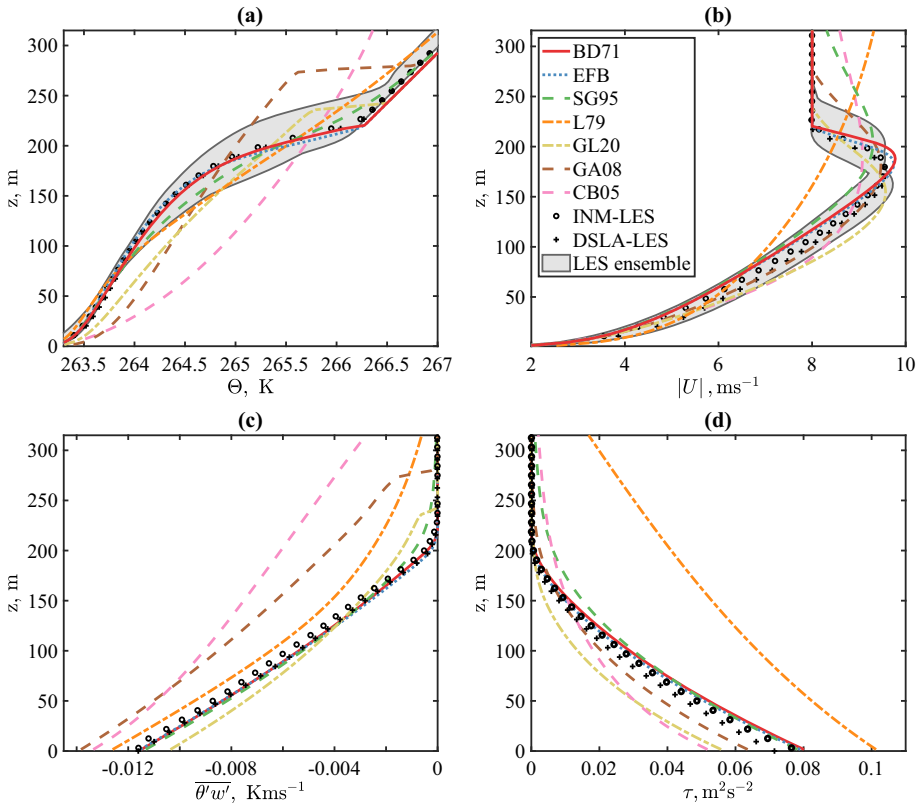


Fig. 2 Profiles of **a** θ , **b** $|U|$, **c** $\overline{\theta'w'}$ and **d** τ from single column models in GABLS1 experiment, for legend key see Table 1. (*INM-LES*) denotes LES data from INM RAS model (Glazunov 2014a), (*DSLA-LES*) denotes data from LES used in Kadantsev et al. (2021). Grey shading denotes model spread, i.e., minimum and maximum value at each vertical level from the ensemble of models with 3.125 m resolution from Beare et al. (2006), data obtained from <https://gabls.metoffice.com>. The profiles are obtained by averaging over last hour of experiment

Figure 2 demonstrates profiles of potential temperature θ , wind speed $|U|$, kinematic heat flux $\overline{\theta'w'}$ and momentum flux τ averaged over the last hour of the experiment. The difference between the BD71 and EFB closures is very small in mean profiles, but is more noticeable for the turbulent fluxes, and both of them are closer to LES data than others. The SG95 closure shows issue with reproducing narrow jet in velocity profile, but produces temperature profile similar to BD71 and EFB. One can also notice that closures with non-linear @ @dimensionless velocity gradient (GA07, GL20, CB05 and L79) significantly differ from the closures EFB, SG95 and BD71, which assume linear velocity gradient, and LES data, this is especially evident for the CB05 closure. At the same time, the greatest error both in mean and flux profiles is given by the closure based on Louis (1979).

4.2 Very Stable Boundary Layer Case

To test first order closures in the case of very stable ABL (VSBL), experiments were performed according to the van der Linden et al. (2019) setup, which corresponds to extreme surface cooling during the Antarctic winter. In general, this formulation does not differ much

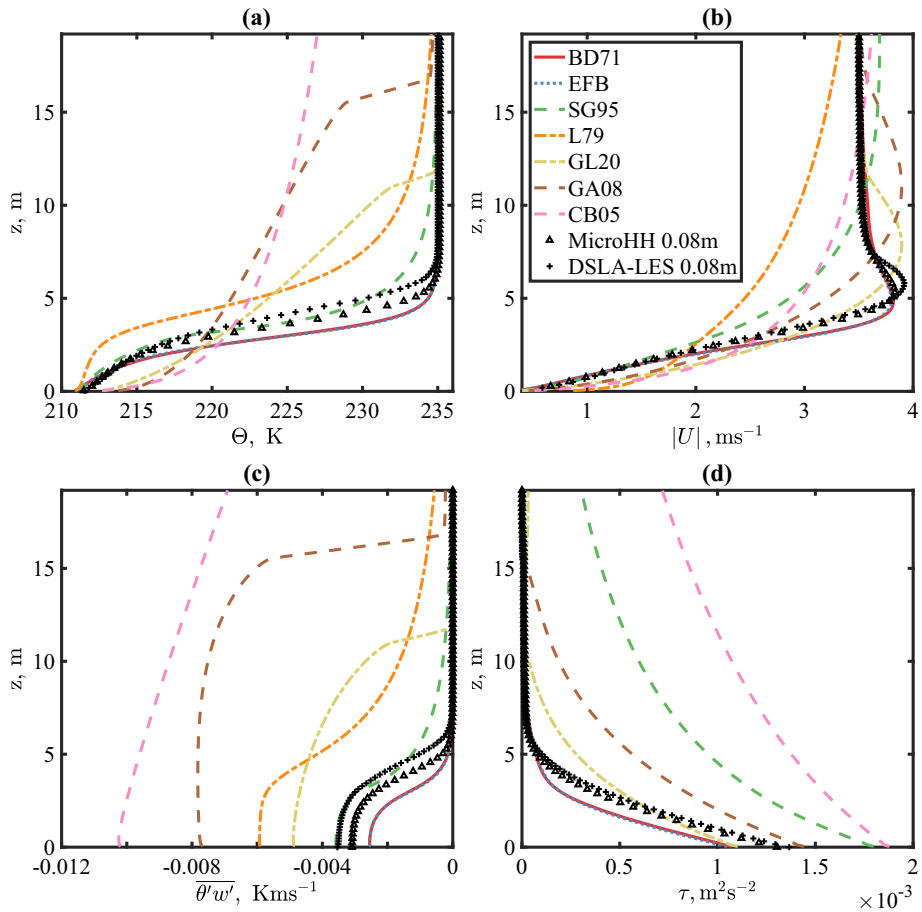


Fig. 3 Profiles of **a** θ , **b** $|U|$, **c** $\overline{\theta'w'}$ and **d** τ from single column simulations of VSBL experiment, for legend key see Table 1. Triangles and crosses represent LES data from van der Linden et al. (2019) and DSLA-LES respectively, averaged over the last hour of the experiment

from GABLS1, except for an increase in the surface cooling rate by a factor of 16 to 4 K s^{-1} after which the surface temperature was kept constant for a significant period (16.75 h) of time. Also one more external forcing was added to the temperature equation in the form of large-scale vertical advection (subsidence), which, on average, contributed to an increase in the temperature gradient in the top part of the ABL. The heat flux profile in this experiment is very different from the linear one.

The simulation results as well as the LES reference profiles (for MicroHH LES from van der Linden et al. (2019) and DSLA-LES) are shown in Fig. 3. In general, the conclusions drawn for the case of weaker stability of GABLS1 can be reiterated in relation to this experiment, but a relatively large spread between the one-dimensional models is worth noting. Thus, the difference in the mean profiles for the BD71, EFB, SG95 closures significantly increases compared to GABLS1, which was most likely due to the difference in closures behavior in the region of strong stability, in particular SG95 and BD71 provide more extensive mixing there. The SG95 also fails to reproduce the jet in this experiment. A further difference is

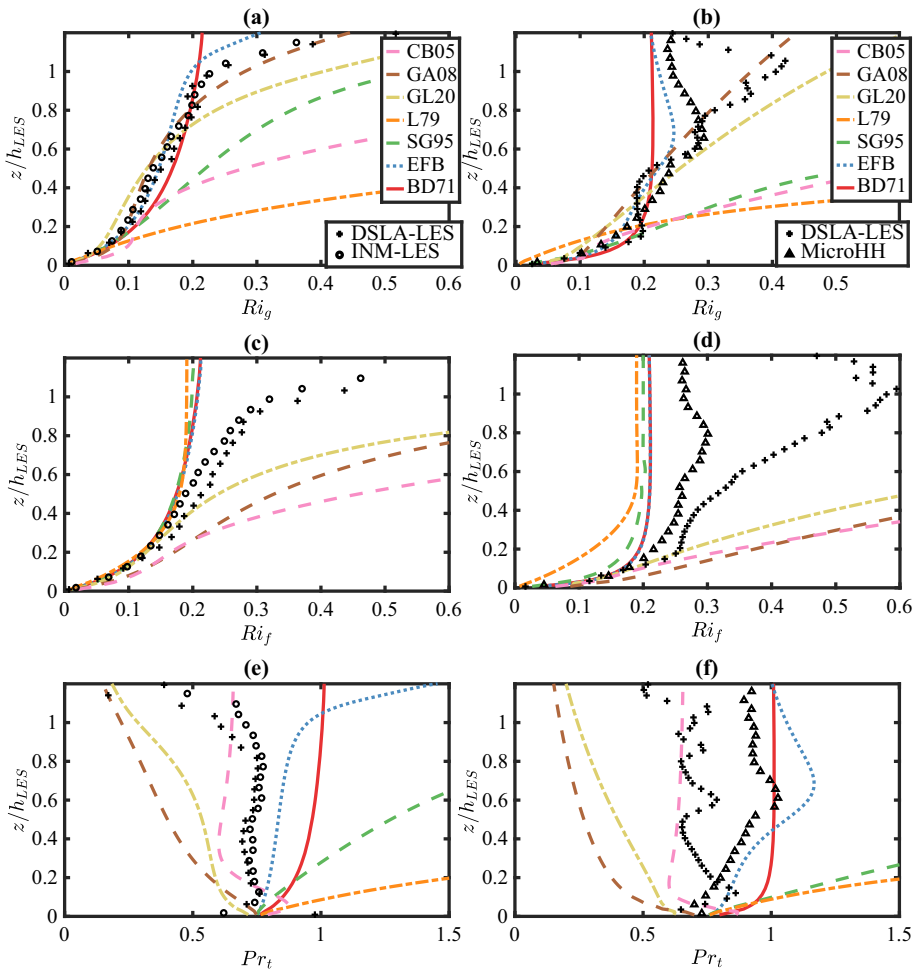


Fig. 4 Profiles of **a, b** Ri_g , **(c,d)** Ri_f , **e, f** Pr_t obtained as a result of single-column experiments for (*left column*) GABLS1 case and (*right column*) VSBL case, for the legend see Table 1. (*INM-LES*) denotes LES data from INM RAS model, (*LES-DSLA*) denotes LES data from LES model with dynamic Smagorinsky and Lagrangian averaging procedures for closure, (*MicroHH LES*)—data of MicroHH LES model simulations from van der Linden et al. (2019). The profiles are obtained by averaging over last hour of experiment

that of all schemes with non-linear velocity gradients, the GL20 scheme shows the best and relatively good agreement with LES with respect to the wind profile and momentum fluxes.

A comparison of the Ri_g , Ri_f and Pr_t profiles for both experiments is shown in Fig. 4. The flux Richardson number is derived from the LES total fluxes (comprised of both the resolved and the “subgrid” flux), and the Prandtl number is calculated as $Pr_t = Ri_g Ri_f^{-1}$. These results corroborate the behavior observed in Fig. 1, but in a form that highlights the dependence on z/h and realized local stability in the closures. That is, the first order closures profiles are all close to LES near the surface and diverge in the outer ABL, and all single column models are closer to LES in the GABLS1 case. Closures that limit Ri_f by their design (L79,SG95, BD71 and EFB) produce near Ri_{fc} values in VSBL experiment and to a lesser extent in GABLS1 case, however from the LES data only MicroHH show a similar behavior. The spread between

the LES models themselves is larger in VSBL experiment than that in GABLS1 experiment for both Ri_g and Ri_f profiles. As Fig. 4e, f show there is little overlap for Pr_t profiles in BD71 and EFB closures despite the very close profiles of wind speed and potential temperature they produce for both weakly and strongly stratified cases in Figs. 2 and 3. This difference corresponds to smaller change in resulting Ri_g profiles. One of the reasons for this might be that these closures operate at close to Ri_{fc} values (which are equal for both closures) in the upper part of the ABL. The main dissimilarities in the results for Pr_t occur at the top of the ABL, where turbulent fluxes are already small and cannot affect mean stability (Ri_g) greatly.

4.3 Evaluation of the Surface Flux Schemes

As noted earlier, generalizing some sets of local dimensionless gradient functions to the entire boundary layer can give significant errors in one-dimensional models if these functions implicitly contain information about the dependence of fluxes on the dimensionless height z/h . However, the same circumstance can give an advantage when using these integrated functions for calculating surface fluxes. On the one hand, the surface layer assumption is violated further with increasing distance from the surface and so will the error in estimated surface fluxes. On the other hand information about the z/h dependence, implicitly introduced into the integral functions, can mitigate this increase in error and extend the range of heights z in which a particular surface flux scheme is applicable. One can try to test this hypothesis using LES data.

The calculation of surface heat and momentum fluxes using bulk formulae can be briefly described as follows: the functions of dimensionless gradients (7) and (8) are integrated under the assumption that the fluxes and Obukhov’s scale L are constant with height, thus forming a system of equations for u_{*s} , θ_{*s} , and L . Then, one can calculate the heat and momentum fluxes near the surface $\overline{\theta'w'_s} = \theta_{*s}u_{*s}$, $\tau_s = u_{*s}^2$:

$$u_{*s} = \frac{(|U(z)| - |U_s|) \kappa}{\Psi_m(z/L) - \Psi_m(z_0/L)}, \tag{35}$$

$$\theta_{*s} = \frac{(\theta(z) - \theta_s) \kappa}{\Psi_h(z/L) - \Psi_h(z_{0t}/L)}, \tag{36}$$

$$L = \frac{u_{*s}^2}{\beta \kappa \theta_{*s}}, \tag{37}$$

where Ψ_m and Ψ_h are the integral universal functions, obtained from ϕ_m and ϕ_h .

External parameters for this system of equations are the values of wind velocity $U(z)$ and temperature $\theta(z)$ at the height z , their values at the surface U_s, θ_s and characteristics of the surface z_0, z_{0t} . All external parameters can be obtained from the LES data for the considered above experiments GABLS1 and VSBL.

Figure 5 shows the surface heat and momentum fluxes calculated from (35)–(37) using all the universal functions considered. These fluxes are shown as dependent on z/h and normalized to the corresponding surface fluxes obtained from LES data, which are supposed to be the true reference data. In this way, we mimic the behavior of the surface fluxes schemes when the values of velocity and temperature at some height z are known, but the variances of the fluxes within the underlying layer are neglected. The deviation of each curve from unity on the horizontal axis shows the relative error of the corresponding scheme and thus indicates its applicability or inapplicability at different distances from the surface.

In Fig. 5 it can be seen that for the GABLS1 experiment with a weakly stable ABL, most of the surface schemes estimate the heat flux well regardless of the dimensionless height z/h ,

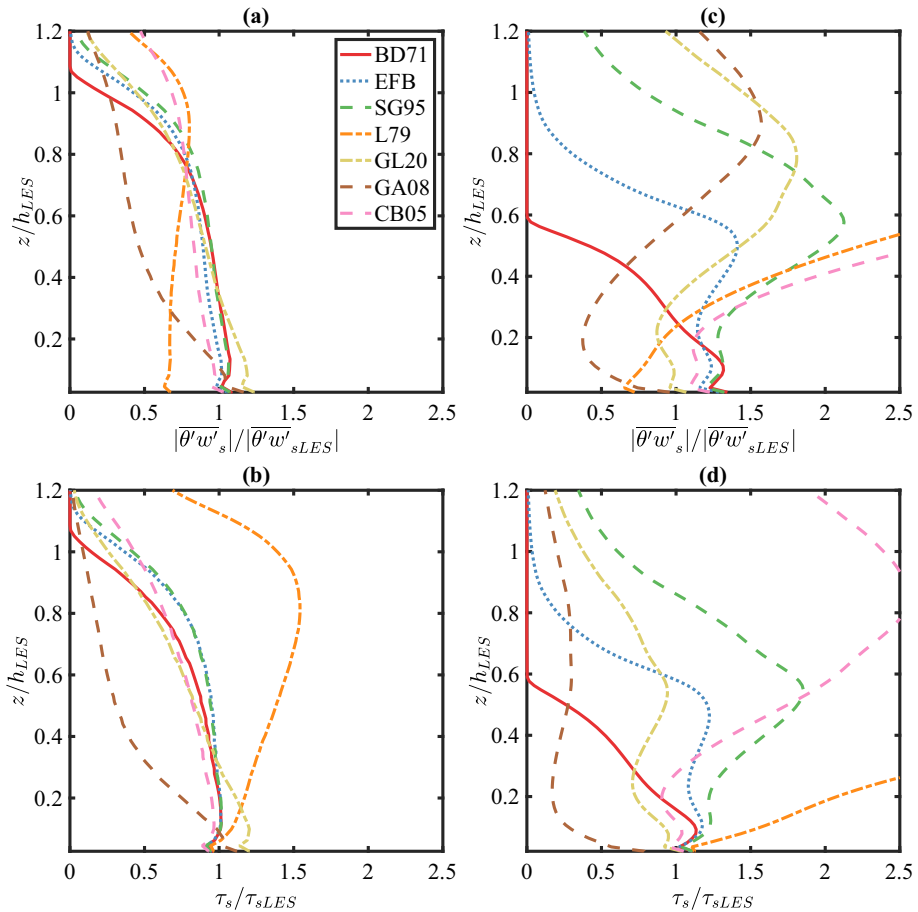


Fig. 5 Profiles of the ratios of the surface kinematic heat flux **a, b** and momentum flux **c, d** calculated by corresponding model bulk formulae to the surface fluxes according to LES simulations data (from DSLA-LES results) in the experiments GABLS1 (Cuxart et al. 2006) (*left column*) and VSBL (van der Linden et al. 2019) (*right column*). The profiles are obtained by averaging over last hour of experiment. Bulk formulas in the legend of this figure are integrated versions of their counterparts in Table 1

but for the momentum flux Louis scheme gives a significant overestimation with height. For the ABL with higher stability in the VSBL experiment, all schemes are not able to correctly estimate the fluxes in the upper half of the ABL $z/h > 0.5$. The closest to unity in lower ABL is EFB closure, however its reproduced momentum flux vanishes quickly in the upper part of the boundary layer. GL20 scheme follows closely and CB05, SG95 and L79 on the other hand perform worse, but keep reproducing non zero momentum flux in the entire ABL, which means their application will not lead to decoupling when used on coarse grid for this stability. This implies that if these surface schemes were to be applied in the GCM model away from the surface layer (i.e., the lowest vertical grid cell was in the $z/h > 0.5$ region of ABL) it will still produce some momentum flux.

5 Conclusions

In this study we conducted an evaluation of different first order schemes with data from LES experiments. The considered schemes were constructed based on generalized MOST following the literature by assuming its local validity. It is shown that derived stability functions and first order closures, which utilize linear velocity dimensionless gradient, provide good agreement with LES data. In particular, the best agreement with the LES data was obtained with Businger et al. (1971) and Zilitinkevich et al. (2013) closures, followed by Schumann and Gerz (1995) based closure. All other closures produce too strong mixing and thus overestimate the ABL height. The degree of overestimation differs from scheme to scheme and depending on the considered property not always the same scheme is superior. However the most disagreement with LES is clearly shown by the Louis (1979) scheme. These results appear to be more pronounced for the VSBL experiment than for weakly stable conditions. One point to note here is that the comparison discussed above represents the application of single column models in favorable conditions from numerical perspective. This means the 1D model was run with very high resolution and with much smaller time steps than those actually utilized in climate and weather prediction models.

We emphasize that here we perform a comparison between closures. The numerical aspects of vertical diffusion parameterizations in global circulation models should be treated as separate issue and evaluated differently. We believe that this study cannot suffice for a definitive answer or even clear recommendation for functions to use or not to use in GCMs. In particular because of interference of ABL scheme with a number of factors such as specific implementation features, numerical approximation errors, other components of GCM and their parameter ranges, there is no guarantee for a particular set of universal functions to perform well in a particular GCM. Therefore, an evaluation of the universal functions performance in GCMs is needed, which warrants a separate study.

The applicability of the considered universal functions for the construction of “bulk formulas” was evaluated. The mean velocity and temperature profiles obtained in LES were used as reference data for calculating surface heat and momentum fluxes. Such setup showcases the behavior of surface scheme when one assumes that above the surface the ABL is represented correctly by the ABL turbulent diffusion scheme. In the case of weakly stratified ABL most surface schemes show good results up to 0.8 of ABL height except for functions proposed in Louis (1979). For very stable ABL surface schemes based on linear dimensionless velocity gradients will produce diminishing fluxes if integrated above half of the ABL, and functions based on Grachev et al. (2007) and Gryanik et al. (2020) will have this region extended to the entire ABL. On the other hand long-tailed functions such as Cheng and Brutsaert (2005) and Louis (1979), will overestimate surface fluxes greatly. This in turn may be a desirable feature for implementation in climate and weather forecast models to prevent decoupling of the ABL from the underlying surface on coarse vertical grids.

Finally, we stress that most of the considered closures had been developed for the surface layer and applying them in the entire ABL leaves the region for which they were defined. However, the presented strategy for their extension might be useful for their future test in climate and weather prediction models and such test are recommended for a large variety of functions to better understand their impact on a larger scale.

Acknowledgements This paper is dedicated to the memory of Sergej Sergeevich Zilitinkevich. His research, well-known and highly regarded in the community (for a great summary see Baklanov et al. 2021), initiated a fundamental rethinking of the planetary boundary layer theory. We are deeply grateful for the discussions we had over the last decade on understanding of turbulent mixing in stratified flows, which sparked our interest for this area of research. for the LES experiments of GABLS1 and VSBL and the Russian Science Foundation

project (N^o 21-71-30003) for the development of LES model. The sensitivity analysis and closure development were performed with support of Russian Science Foundation (RSF N^o 20-17-00190). The paper was published with the financial support of the Ministry of Education and Science of the Russian Federation as part of the program of the Moscow Center for Fundamental and Applied Mathematics under the agreement N^o 075-15-2022-284. Authors would like to thank Steven van der Linden for providing LES data of MicroHH model for Dome-C based experiments and GABLS1-consortium for making the results of their LES available. Authors gratefully acknowledge the three anonymous reviewers for very helpful comments and valuable suggestions to increase clarity of this paper.

Data Availability The datasets generated during and/or analyzed during the current study are available from the corresponding author on reasonable request.

Appendix 1: Relations of Ri_g and Stability Parameter ζ

For the solution of the system (1)–(10), an expression for ζ through mean velocity and temperature profiles, using Eq. (13) is needed. For some of the closures this could be done analytically (see below for BD71 and EFB, or using Eq. (22) for SG95). Other closures require some sort of iterative procedure. The simplest one to derive is an iteration method of the form:

$$\zeta_{n+1} = \frac{Ri_g \phi_m^2(\zeta_n)}{\phi_h(\zeta_n)}. \tag{38}$$

This method seems to work relatively well and more complicated Newton-Raphson method seems to only marginally improve computational cost.

Linear dimensionless gradients

To solve the closure for linear dimensionless gradients substituting (14) and (15) into (13) gives:

$$Ri_g = \frac{\zeta \phi_h}{\phi_m^2} = \frac{Pr_{t0} \zeta (1 + C_h \zeta)}{(1 + C_m \zeta)^2}, \tag{39}$$

one can rewrite it as a quadratic equation in relation ζ :

$$(Pr_{t0} C_h - C_m^2 Ri_g) \zeta^2 + (Pr_{t0} - 2C_m Ri_g) \zeta - Ri_g = 0 \tag{40}$$

Assuming non-negativity of Ri_g , and typical range of C_m and C_h ($C_m \leq C_h$), after some calculus one can show that (40) has a non-negative solution. This would be branch of the root:

$$\zeta^+ = \frac{2C_m Ri_g - Pr_{t0} + \sqrt{4(Pr_{t0} C_h - C_m) Ri_g + Pr_{t0}^2}}{2(Pr_{t0} C_h - C_m^2 Ri_g)}, \tag{41}$$

which becomes non-negative at $Ri_g = 0$. In simplified case of $C_m = Pr_{t0} C_h$, this solution is reduced to $\zeta = \frac{Ri_g}{1 - C_m Ri_g}$, which one can find in Soloviev et al. (2001).

EFB Closure

For the EFB closure substituting Eq. (24) into Eq. (21) gives:

$$Ri_g = \frac{\left(\frac{C_\tau}{C_F}\right) (A_{z0} + C_a \zeta) (1 + (C_m - 1) \zeta) \zeta}{(1 + C_m \zeta) \left(C_2 (A_{z0} + C_a \zeta) (1 + (C_m - 1) \zeta) - C_1 \zeta \left(1 + \frac{C_a}{A_{z\infty}} \zeta\right)\right)}, \tag{42}$$

which leads to a cubic equation relative to ζ :

$$(g_1 - h_1) \zeta^3 + (g_2 - h_2) \zeta^2 + (g_3 - h_3) \zeta + g_4 = 0. \tag{43}$$

where:

$$h_1 = \frac{C_\tau}{C_F} C_a (C_m - 1), \tag{44}$$

$$h_2 = \frac{C_\tau}{C_F} (A_{z0} (C_m - 1) + C_a), \tag{45}$$

$$h_3 = \frac{C_\tau}{C_F} A_{z0}, \tag{46}$$

and:

$$g_1 = Ri_g C_m C'_1, \quad g_2 = Ri_g (C'_1 + C_m C'_2), \tag{47}$$

$$g_3 = Ri_g (C'_2 + C_m C'_3), \quad g_4 = Ri_g C'_3 \tag{48}$$

$$C'_1 = C_a \left(C_2 (C_m - 1) - \frac{C_1}{A_{z\infty}} \right), \tag{49}$$

$$C'_2 = C_2 (A_{z0} (C_m - 1) + C_a) - C_1, \tag{50}$$

$$C'_3 = C_2 A_{z0}. \tag{51}$$

Here we utilize the constants from Zilitinkevich et al. (2013):

$$C_P = 0.62, \quad C_m = 5.0, \tag{52}$$

$$C_\theta = 0.76, \quad C_\nabla = 0.78, \tag{53}$$

$$C_\tau = 0.15, \quad C_F = C_\tau / [(1 + C_\nabla) Pr_{t0}], \tag{54}$$

and:

$$A_{z\infty} = 0.0209, \quad A_{z0} = 0.2, \quad C_a = 0.003. \tag{55}$$

A_z is approximated by:

$$A_z = \frac{A_{z0} + C_a \frac{z}{L}}{1 + \frac{C_a}{A_{z\infty}} \frac{z}{L}}. \tag{56}$$

The physically meaningful root can be found by:

$$\zeta = \begin{cases} \sqrt[3]{4} (q^2 - \sqrt{-\Delta})^{1/6} \cos\left(\frac{1}{3} \text{atan2}(\sqrt{-\Delta}, -q)\right) - \frac{b}{3}, & \Delta < 0, \\ \sqrt[3]{\left(\frac{-q + \sqrt{\Delta}}{2}\right)} + \sqrt[3]{\left(\frac{-q - \sqrt{\Delta}}{2}\right)} - \frac{b}{3}, & \Delta > 0, \end{cases} \tag{57}$$

where $\text{atan2}(\alpha, \beta)$ is the four-quadrant inverse tangent function, and:

$$q = \left(\frac{2}{27} \left(\frac{g_2 - h_2}{g_1 - h_1} \right)^2 - \frac{1}{3} \frac{g_3 - h_3}{g_1 - h_1} \right) \frac{g_2 - h_2}{g_1 - h_1} + \frac{g_4}{g_1 - h_1},$$

$$\Delta = q^2 + \frac{4}{27} \left(\frac{-1}{3} \frac{g_2 - h_2}{g_1 - h_1} + \frac{g_2 - h_2}{g_1 - h_1} \right)^3,$$

$$b = \frac{1}{3} \frac{g_2 - h_2}{g_1 - h_1}. \tag{58}$$

References

- Baklanov A, Esau I, Mironov D (2021) Sergej Zilitinkevich (13.4. 1936–15.2. 2021). Springer
- Basu S, Holtslag AA (2021) Turbulent Prandtl number and characteristic length scales in stably stratified flows: steady-state analytical solutions. *Environ Fluid Mech* 21(6):1273–1302
- Basu S, Porté-Agel F (2006) Large-eddy simulation of stably stratified atmospheric boundary layer turbulence: a scale-dependent dynamic modeling approach. *J Atmos Sci* 63(8):2074–2091
- Beare RJ, Macvean MK, Holtslag AA, Cuxart J, Esau I, Golaz JC, Jimenez MA, Khairoutdinov M, Kosovic B, Lewellen D et al (2006) An intercomparison of large-eddy simulations of the stable boundary layer. *Boundary-Layer Meteorol* 118(2):247–272
- Businger JA, Wyngaard JC, Izumi Y, Bradley EF (1971) Flux-profile relationships in the atmospheric surface layer. *J Atmos Sci* 28(2):181–189
- Cheng Y, Brutsaert W (2005) Flux-profile relationships for wind speed and temperature in the stable atmospheric boundary layer. *Boundary-Layer Meteorol* 114(3):519–538
- Couvreur F, Bazile E, Rodier Q, Maronga B, Matheou G, Chinita MJ, Edwards J, van Stratum BJ, van Heerwaarden CC, Huang J et al (2020) Intercomparison of large-eddy simulations of the Antarctic boundary layer for very stable stratification. *Boundary-Layer Meteorol* 176(3):369–400
- Cuxart J, Holtslag AA, Beare RJ, Bazile E, Beljaars A, Cheng A, Conangla L, Ek M, Freedman F, Hamdi R et al (2006) Single-column model intercomparison for a stably stratified atmospheric boundary layer. *Boundary-Layer Meteorol* 118(2):273–303
- Deardorff JW (1970) Convective velocity and temperature scales for the unstable planetary boundary layer and for Rayleigh convection. *J Atmos Sci* 27(8):1211–1213
- Derbyshire S (1999) Stable boundary-layer modelling: established approaches and beyond. *Boundary-Layer Meteorol* 90(3):423–446
- Dufresne JL, Foujols MA, Denvil S, Caubel A, Marti O, Aumont O, Balkanski Y, Bekki S, Bellenger H, Benschila R et al (2013) Climate change projections using the IPSL-CM5 earth system model: from CMIP3 to CMIP5. *Clim Dyn* 40(9):2123–2165
- Dyer A (1974) A review of flux-profile relationships. *Boundary-Layer Meteorol* 7(3):363–372
- Emeis S (2014) Current issues in wind energy meteorology. *Meteorol Appl* 21(4):803–819
- Esau IN (2008) Formulation of the planetary boundary layer feedback in the Earth's climate system. *Comput Technol* 13(S3):90–103
- Garratt J, Wilczak J, Holtslag A, Schmid HP, Grachev A, Beljaars A, Foken T, Chen F, Fairall C, Hicks B et al (2020) Commentaries on top-cited boundary-layer meteorology articles. *Boundary-Layer Meteorol* 177(2):169–188
- Genthon C, Six D, Gallée H, Grigioni P, Pellegrini A (2013) Two years of atmospheric boundary layer observations on a 45-m tower at Dome C on the Antarctic plateau. *J Geophys Res Atmos* 118(8):3218–3232
- Glazunov A (2014) Numerical modeling of turbulent flows over an urban-type surface: computations for neutral stratification. *Izv Atmos Ocean Phys* 50(2):134–142
- Glazunov A (2014) Numerical simulation of stably stratified turbulent flows over an urban surface: spectra and scales and parameterization of temperature and wind-velocity profiles. *Izv Atmos Ocean Phys* 50(4):356–368
- Glazunov A, Rannik Ü, Stepanenko V, Lykosov V, Auvinen M, Vesala T, Mammarella I (2016) Large-eddy simulation and stochastic modeling of Lagrangian particles for footprint determination in the stable boundary layer. *Geosci Model Dev* 9(9):2925–2949
- Glazunov A, Mortikov E, Barskov K, Kadantsev E, Zilitinkevich S (2019) Layered structure of stably stratified turbulent shear flows. *Izv Atmos Ocean Phys* 55(4):312–323
- Grachev AA, Andreas EL, Fairall CW, Guest PS, Persson POG (2007) SHEBA flux-profile relationships in the stable atmospheric boundary layer. *Boundary-Layer Meteorol* 124(3):315–333
- Grachev AA, Andreas EL, Fairall CW, Guest PS, Persson POG (2008) Turbulent measurements in the stable atmospheric boundary layer during SHEBA: ten years after. *Acta Geophys* 56(1):142–166
- Gryanik VM, Lüpkes C (2022) A package of momentum and heat transfer coefficients for the stable surface layer extended by new coefficients over sea ice. *Boundary-Layer Meteorol* 1–32. <https://doi.org/10.1007/10546-022-00730-9>
- Gryanik VM, Lüpkes C, Grachev A, Sidorenko D (2020) New modified and extended stability functions for the stable boundary layer based on SHEBA and parametrizations of bulk transfer coefficients for climate models. *J Atmos Sci* 77(8):2687
- Holtslag A, Svensson G, Baas P, Basu S, Beare B, Beljaars A, Bosveld F, Cuxart J, Lindvall J, Steeneveld G et al (2013) Stable atmospheric boundary layers and diurnal cycles: challenges for weather and climate models. *Bull Am Meteorol Soc* 94(11):1691–1706

- Kadantsev E, Mortikov E, Zilitinkevich S (2021) The resistance law for stably stratified atmospheric planetary boundary layers. *Q J R Meteorol Soc* 147(737):2233–2243
- Katul GG, Porporato A, Shah S, Bou-Zeid E (2014) Two phenomenological constants explain similarity laws in stably stratified turbulence. *Phys Rev E* 89(2):023007
- Louis JF (1979) A parametric model of vertical eddy fluxes in the atmosphere. *Boundary-Layer Meteorol* 17(2):187–202
- Louis J, Tiedtke M, Geleyn J (1982) A short history of the operational PBL-Parameterization of ECMWF. In: Workshop on planetary boundary layer parameterization
- Maronga B, Li D (2022) An investigation of the grid sensitivity in large-eddy simulations of the stable boundary layer. *Boundary-Layer Meteorol* 182(2):251–273
- Meneveau C, Lund TS, Cabot WH (1996) A Lagrangian dynamic subgrid-scale model of turbulence. *J Fluid Mech* 319:353–385
- Monin A, Yaglom A (1971) *Statistical fluid mechanics, vol 1*. MIT Press, Cambridge/Mass
- Mortikov E, Glazunov A, Debolskiy A, Lykosov V, Zilitinkevich S (2019) Modeling of the dissipation rate of turbulent kinetic energy. *Doklady earth sciences*, vol 489. Springer, pp 1440–1443
- Nieuwstadt FT (1984) The turbulent structure of the stable, nocturnal boundary layer. *J Atmos Sci* 41(14):2202–2216
- Petenko I, Argentini S, Casasanta G, Genthon C, Kallistratova M (2019) Stable surface-based turbulent layer during the polar winter at Dome C, Antarctica: sodar and in situ observations. *Boundary-Layer Meteorol* 171(1):101–128
- Pleim J, Gilliam R, Godowitch J (2010) Evaluation of PBL models compared to GABLS experiments and testing meteorology and air quality models. In: 19th symposium on boundary layers and turbulence conference proceedings
- Schumann U, Gerz T (1995) Turbulent mixing in stably stratified shear flows. *J Appl Meteorol* 34(1):33–48
- Soloviev A, Lukas R, Hacker P (2001) An approach to parameterization of the oceanic turbulent boundary layer in the western Pacific warm pool. *J Geophys Res Oceans* 106(C3):4421–4435
- Sterk H, Steeneveld G, Holtslag A (2012) Unravelling the role of turbulent mixing, land surface coupling and radiation in a coupled GABLS1 experiment. In: Proceedings of the workshop on diurnal cycles and the stable boundary layer, Reading, 7–10 Nov 2011, pp 251–251
- Stretch D, Rottman J, Nomura K, Venayagamoorthy S (2001) Transient mixing events in stably stratified turbulence. In: 14th Australasian fluid mechanics conference. Adelaide, Australia, pp 10–14
- Sullivan PP, Weil JC, Patton EG, Jonker HJ, Mironov DV (2016) Turbulent winds and temperature fronts in large-eddy simulations of the stable atmospheric boundary layer. *J Atmos Sci* 73(4):1815–1840
- Svensson G, Holtslag AA (2009) Analysis of model results for the turning of the wind and related momentum fluxes in the stable boundary layer. *Boundary-Layer Meteorol* 132(2):261–277
- Tkachenko E, Debolskiy A, Mortikov E (2021) Intercomparison of subgrid scale models in large-eddy simulation of sunset atmospheric boundary layer turbulence: computational aspects. *Lobachevskii J Math* 42(7):1580–1595
- van der Linden SJ, Edwards JM, van Heerwaarden CC, Vignon E, Genthon C, Petenko I, Baas P, Jonker HJ, van de Wiel BJ (2019) Large-eddy simulations of the steady wintertime Antarctic boundary layer. *Boundary-Layer Meteorol* 173(2):165–192
- Voltaire A, Sanchez-Gomez E, Salas y Mélia D, Decharme B, Cassou C, Sénési S, Valcke S, Beau I, Alias A, Chevallier M, et al (2013) The CNRM-CM5.1. global climate model: description and basic evaluation. *Clim Dyn* 40(9):2091–2121
- Volodin E, Mortikov E, Kostykin S, Galin VY, Lykosov V, Gritsun A, Diansky N, Gusev A, Iakovlev N (2017) Simulation of the present-day climate with the climate model inmcm5. *Clim Dyn* 49(11):3715–3734
- Zilitinkevich S, Baklanov A (2002) Calculation of the height of the stable boundary layer in practical applications. *Boundary-Layer Meteorol* 105(3):389–409
- Zilitinkevich S, Elperin T, Kleerorin N, Rogachevskii I, Esau I (2013) A hierarchy of energy-and flux-budget (EFB) turbulence closure models for stably-stratified geophysical flows. *Boundary-Layer Meteorol* 146(3):341–373
- Zilitinkevich S, Druzhinin O, Glazunov A, Kadantsev E, Mortikov E, Repina I, Troitskaya Y et al (2019) Dissipation rate of turbulent kinetic energy in stably stratified sheared flows. *Atmos Chem Phys* 19(4):2489

Publisher's Note Springer Nature remains neutral with regard to jurisdictional claims in published maps and institutional affiliations.

Springer Nature or its licensor (e.g. a society or other partner) holds exclusive rights to this article under a publishing agreement with the author(s) or other rightsholder(s); author self-archiving of the accepted manuscript version of this article is solely governed by the terms of such publishing agreement and applicable law.